DOI: 10.1002/ejic.200700279

Hafnium Oxide Doped Mesostructured Silica Films

Ralf Supplit,[a] Nicola Hüsing,*[b] Silvia Gross,[c] Sigrid Bernstorff,[d] and Michael Puchberger[a]

Keywords: Mesostructured films / Ligand-assisted templating / Self-assembly / Surfactants

Hafnium oxide doped silica films with ordered mesostructures were produced with hafnium:silicon ratios between 1:60 and 1:6. A surfactant–hafnium alkoxide complex was synthesized and used as a template in a sol–gel dip-coating process. Face-centred orthorhombic, 2D centred rectangular and lamellar films were formed by evaporation-induced self-assembly (EISA). The influence of subsequent heat treatment was studied by GISAXS and TEM. The surface and in-depth molecular composition of the films was studied by XPS.

Introduction

Hafnium dioxide is a ceramic material characterized by high thermal and chemical stability, high dielectric constant, good mechanical strength, catalytic properties and low electrical conductivity.[1–3] Stable porous mesostructured hafnium oxide was successfully synthesized by the groups of Sayari and Stucky by applying a surfactant templating approach[4,5] and, recently, the first mesoporous and even mesostructured thin films of crystalline hafnia were reported by using large nonionic block-copolymer templates as the structure-directing agent.[6,7]

The incorporation of hafnia in silica can lead to a noticeable improvement in the properties of SiO_2, for example for catalytic applications, and at the same time the problems related to the use of pure hafnium dioxide, such as high cost and low specific surface area, can be overcome. Furthermore, the binary HfO_2–SiO_2 system is appealing for the development of high-κ film to overcome limitations in the fabrication of integrated circuits.[8–10] In the past, hafnia–silica systems were developed by using conventional sol–gel processing; however a homogeneous distribution of the Hf- and Si-centres in the matrix is difficult to achieve owing to the different reaction rates of the corresponding alkoxide precursors that often result in phase separation. It is well-known that the reactivity of alkoxide precursors towards hydrolysis and condensation increases dramatically with an increase in the atomic number of the elements with the same valence: for example, silicon alkoxides < titanium alkoxides < hafnium alkoxides. Several strategies were developed to overcome the problems related to these different reactions rates, such as a modified sol–gel process based on the reaction of organically modified hafnium oxoclusters with organofunctional silanes,[11] the pyrolytic conversion of single-source precursors[12] and a chemical solution deposition approach.[13]

Highly porous, mesostructured binary HfO_2–SiO_2 films have – at least to the best of our knowledge – not been reported so far. The aim of this study is to present a synthetic strategy that allows not only precise control over the evolution of the final periodically arranged solid structure in the mixed oxide (HfO_2–SiO_2) thin film, but also a homogeneous distribution of Hf in the silica matrix even for high Hf:Si ratios. Our approach is based on a combination of ligand-assisted templating methods in which the faster reacting alkoxide (Hf-alkoxide) is coordinated to the structure-directing agent – a nonionic surfactant – in combination with a solvent evaporation-induced self-assembly approach for rapid film formation by dip-coating.

Results and Discussion

Hafnium alkoxide/surfactant complexes were formed by the equimolar reaction of hafnium *n*-butoxide with the terminal hydroxyl group of the surfactant Brij-56 ($C_{16}EO_{10}$, decaethyleneglycol hexadecyl ether) (Scheme 1). The resulting complex (Hf–Brij) was analyzed by 2D-NMR spectroscopy.

Figure 1 shows the HSQC spectra of the product (a) compared with the unmodified surfactant (b) and with the pure hafnium butoxide (c). The dotted circle in Figure 1 (a-5) highlights a new peak at δ = 4.20 ppm (^{1}H)/69.2 ppm

[a] Institute of Materials Chemistry, Vienna University of Technology,
Getreidemarkt 9, 1060 Vienna, Austria
[b] Inorganic Chemistry I, University of Ulm,
Albert-Einstein-Allee 11, 89081 Ulm, Germany
Fax: +49-731-5022733
E-mail: nicola.huesing@uni-ulm.de
[c] CNR-ISTM, Department of Chemistry, University of Padua,
Via Marzolo, 1, Padova, Italy
[d] Sincrotone Trieste, Strada Statale 14, Km 163.5, in AREA Science Park,
34012 Basovizza, Trieste, Italy

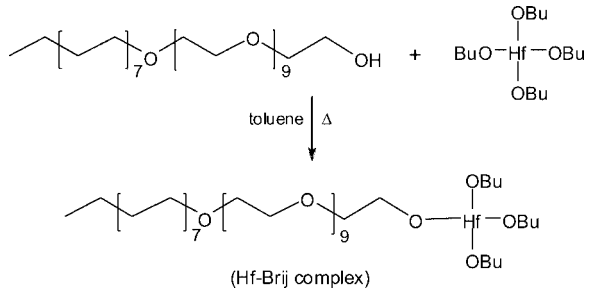

Scheme 1. Synthesis of the Hf–Brij coordination compound.

(^{13}C) that appeared after the reaction of hafnium butoxide with Brij-56, whereas the signal at δ = 4.05 ppm (^{1}H)/ 69.3 ppm (^{13}C) [Figure 1 (a-4)], which was assigned to O-*CH*$_2$ of the butoxy groups, stayed unchanged. The new peak was assigned to the CH_2 group of the surfactant chain that is coordinated to the hafnium through an oxygen bridge. The TOCSY spectrum further shows that this signal correlates only to the CH_2 signal at δ = 3.57 ppm of the surfactant, whereas the signal at δ = 4.05 ppm correlates to signals at δ = 1.55, 1.36 and 0.95 ppm and can therefore be clearly assigned to a butoxy group.

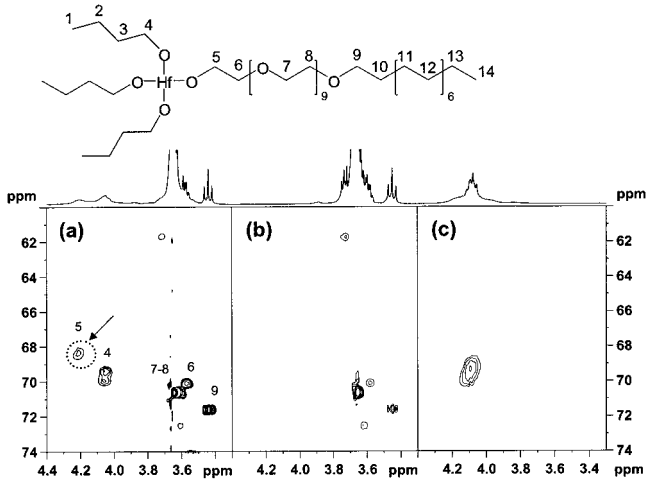

Figure 1. 2D NMR (HSQC) spectra of (a) Hf–Brij-56, (b) Brij-56 and (c) Hf(OBu)$_4$.

The Hf–Brij complex was used as the structure-directing agent in an evaporation-induced self-assembly process (EISA) to form mesostructured thin films (Figure 2).[14] The modified surfactant was added to a prehydrolyzed solution of tetraethoxysilane to form an opalescent sol. Direct addition of hafnium butoxide to such a sol would result in immediate precipitation of hafnia. This shows that the surfactant does not only serve as a structure-directing agent but also acts as an agent to control and slow down the hydrolysis and condensation rate of the alkoxide. Films were prepared by dip-coating from solutions containing different molar ratios (*M*) of the modified surfactant/tetraethoxysilane in otherwise constant composition. The resultant films were labelled Hf–Brij (*M*).

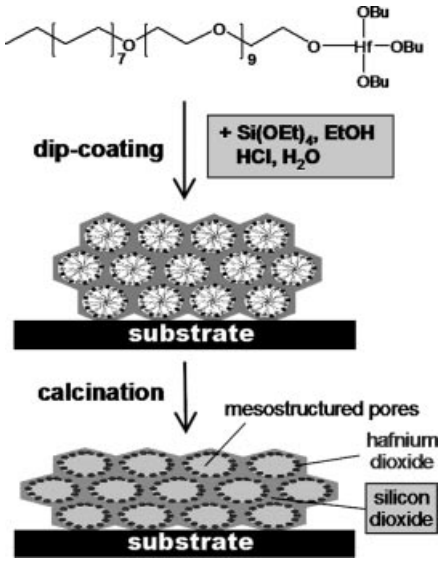

Figure 2. Schematic description of the synthetic strategy towards mesostructured hafnium oxide doped silica films.

The phase diagram of the surfactant Brij-56 shows cubic-spherical micellar, hexagonal, cubic-bicontinuous, lamellar and reversed-cubic-bicontinuous mesophases in surfactant/water mixtures with increasing concentrations of the amphiphile.[15] During the sol–gel process, the silica species replace the position of the water molecules in the hydrophilic regions of the mesophases and the volume fraction ratio of silica to amphiphile can be used to roughly predict the arising mesophases.[16] However, the systems become more complicated when mixed oxide precursors are in use, and the phase diagrams can only be used as a first guideline for the prediction of the accessible structures. When the modified surfactant is removed by calcination, it leaves the transition-metal oxide in the matrix. In this way, a silica film doped with hafnium oxide in periodically arranged mesopores is produced (Figure 2). EXAFS analysis in previous studies showed that this approach yields a molecular dispersion of the transition-metal oxide (titanium or iron) within the silica matrix without the agglomeration to nanoparticles.[17]

In the present study, a sequence of Hf oxide doped films that were prepared with different ratios (*M*) of Hf–Brij/tetraethoxysilane was analyzed by GISAXS (Figure 3). The predominant feature of the diffraction patterns is the formation of diffraction spots rather than rings, which indicates that the films are highly textured. Evaporation-induced self-assembly usually results in films with the densest crystallographic plane of the mesostructure aligned parallel to the substrate.[18] From the phase diagram of Brij-56, micellar cubic and hexagonal mesostructures are expected at low concentrations of the surfactant. During the drying and calcination processes of the films, shrinkage occurred preferentially along the direction normal to the surface plane. Because the mesostructure is aligned with respect to the substrate, this shrinkage is anisotropic and results in distortion of the mesostructure. Body-centred cubic (*Im*3*m*) struc-

tures transform to face-centred orthorhombic (*Fmmm*) and 2D-hexagonal (*P6m*) to 2D centred rectangular mesostructures (*C2mm*).[19–21] In agreement to that, the GISAXS analysis showed that with increasing surfactant concentrations, face-centred orthorhombic ($0.03 < M < 0.06$), 2D-centered rectangular ($M = 0.10$) and lamellar films ($M = 0.17$) were obtained. At a ratio $M = 0.12$, a biphasic film was obtained that consists of 2D-centered rectangular and lamellar mesostructures. We also found biphasic films consisting of face-centred orthorhombic as well as 2D-centered rectangular domains in the concentration range $0.06 < M < 0.10$. The existence of two phases in the same film can be attributed to a concentration gradient and inhomogeneity during EISA or to the presence of two interfaces: solid–liquid and liquid–air.

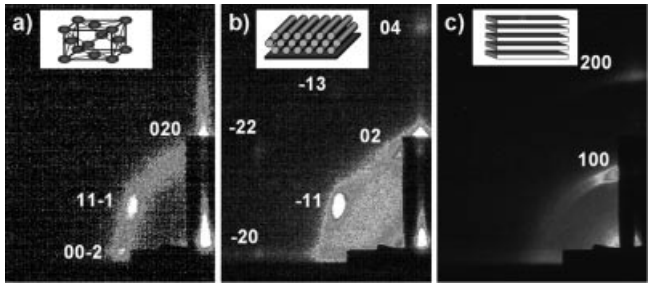

Figure 3. GISAXS pattern for Hf–Brij(0.034), Hf–Brij(0.102), Hf–Brij(0.12) and Hf–Brij(0.17) in the as-deposited state.

No structures that are derived from a bicontinuous cubic mesophase were obtained. Under certain reaction conditions (i.e. aging temperature of 45 °C), the formation of films with this mesostructure was described in the literature.[22]

In contrast, films that were prepared under the same conditions with unmodified Brij-56 did not result in the formation of an orthorhombic mesostructure. The obtained films were disordered ($M < 0.05$), 2D-centered rectangular ($0.05 < M < 0.21$) and lamellar ($0.21 < M < 0.42$). The fact that an additional mesostructure was formed under the same conditions with the hafnium alkoxide/Brij-56 complex can be explained by the larger head group volume of the modified surfactant, which increases the stability of mesostructures with a higher curvature.

The films were successively heat-treated at different temperatures and a GISAXS pattern was recorded after each step (Figure 4). The orthorhombic mesostructure had unit cell parameters of $a = 9.1$, $b = 10.2$ and $c = 12.8$ nm in the as-deposited state. After calcination at 700 °C, shrinkage was observed exclusively along the b direction of the unit cell (perpendicular to the substrate) to give $a = 9.1$, $b = 6.9$ and $c = 12.9$ nm.

TEM analysis (Figure 5) of the calcined (500 °C) sample of Hf–Brij(0.034) confirmed the face-centred orthorhombic mesostructure.

The 2D-centered rectangular GISAXS pattern of Hf–Brij(0.10) (Figure 6) showed unit cell parameters of $a = 6.9$ and $b = 9.6$ nm at 25 °C. After heat treatment to 500 °C, the unit cell parameters are $a = 6.7$ and $b = 6.5$. The shrinkage (30%) occurred as expected and almost exclusively along the direction perpendicular to the substrate plane. Further heat treatment to 700 °C resulted in the destruction of the mesostructure as indicated by a strong decrease in the intensity of the 02 diffraction spot and the disappearance of the –11 and –20 spots, respectively.

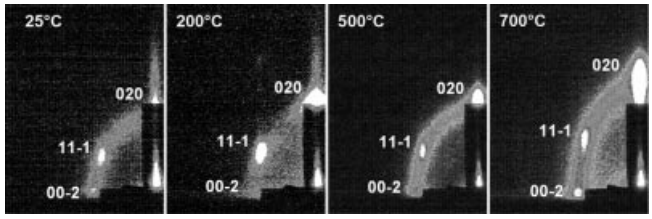

Figure 4. GISAXS series of Hf–Brij(0.034) as-deposited and successively calcined at the indicated temperatures.

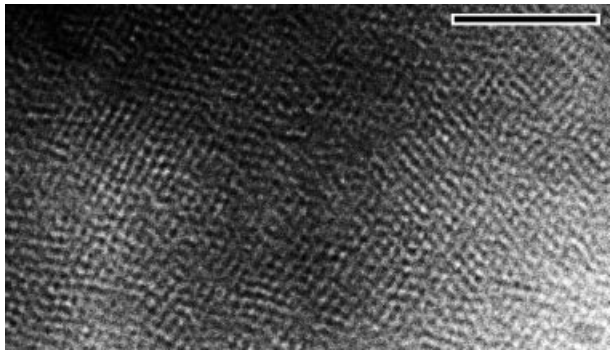

Figure 5. TEM analysis of Hf-Brij(0.034) after calcination at 450 °C; scale bar = 100 nm.

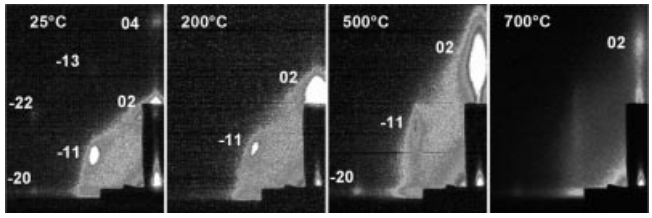

Figure 6. GISAXS series of Hf–Brij(0.10) successively calcined at the indicated temperatures.

TEM analysis of Hf–Brij(0.10) after calcination at 500 °C shows the cylindrical pores of the 2D-centered rectangular mesostructure (Figure 7).

Wide angle XRD (Figure 8) shows an amorphous network below 900 °C. Above that temperature crystallization of tetragonal hafnia occurred and the crystallite size reached approximately 10 nm at 1200 °C.[12]

The surface and in-depth composition of the Hf–Brij(0.12) sample after calcination at 450 °C was analyzed by XPS. The atomic percentages of the different elements of interest (O, Hf, C, Si) were evaluated as a function of the sputtering time, which can in turn be related to the depth of the sample.

In Figure 9 the survey spectra of the Hf–Brij(0.12) samples at the outer surface (a) and after 60 min sputtering (b) are superimposed. As it can be seen, on the surface the

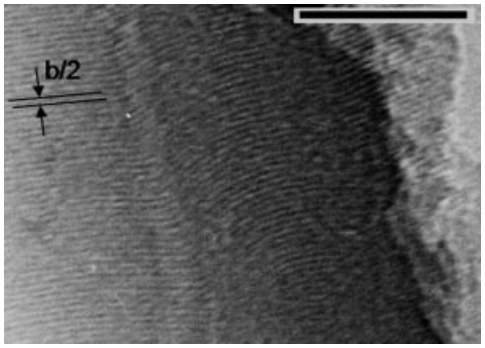

Figure 7. TEM image of Hf–Brij(0.10) after calcination at 500 °C viewed perpendicular to the unit cell *b* axis; scale bar = 100 nm.

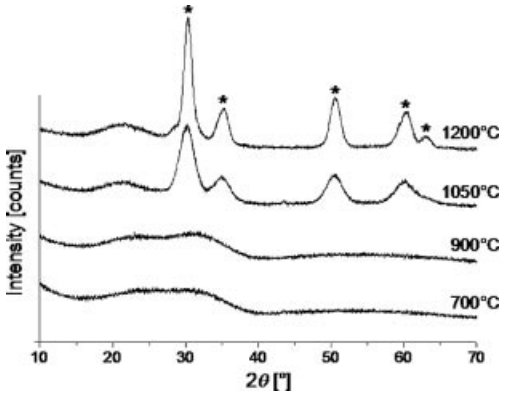

Figure 8. Temperature-dependent X-ray diffraction patterns for Hf–Brij(0.10) calcined at different temperatures. Asterisks indicate the diffraction peaks of the tetragonal hafnia phase.

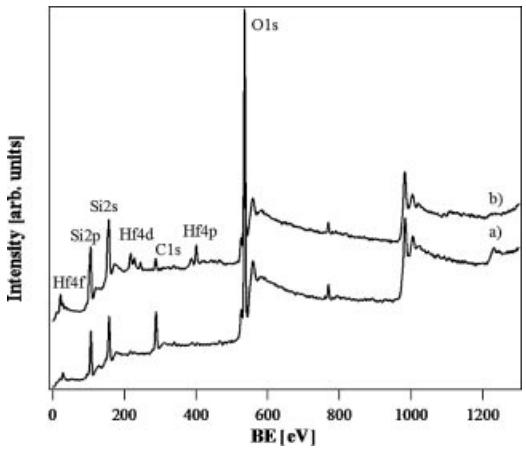

Figure 9. Superimposed survey spectra of the sample before (a) and after (b) 60 min sputtering.

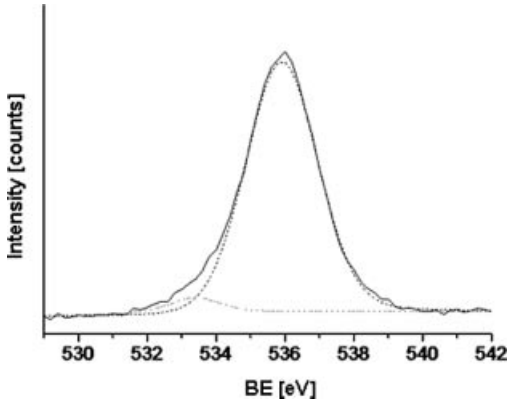

Figure 10. Deconvoluted O1s peak after 20 min sputtering.

peaks corresponding to silicon, carbon and oxygen are distinctly evident, whereas after sputtering the peaks of hafnium could also be detected. Additionally, upon sputtering, a noticeable reduction in the carbon contamination was detected, but carbon was also still present in the inner layers of the film. In addition to the survey spectra, selected spectra of the regions of interest were also acquired. The binding energies (BE) in the annealed samples were corrected for charging effects by assuming for the C1s transition a value typical for adventitious carbon (284.6 eV).[23] As it can be seen in Figure 10, the O1s peak is asymmetric and consists of two components, which could be evidenced after deconvolution. The major contribution whose value is, after charge correction, 532.9 eV, was ascribed to silica, whereas a further component at 530.6 eV (after charge correction), could be ascribed to hafnia, in agreement with the value reported in the literature.[23] Accordingly, the area intensity ratio of the two components is about 11, which is also the detected Si/Hf molar ratio.

As far as the Hf4f peak is concerned, the detected values range in the interval 17.6–18.0 and are higher than the value reported for bulk hafnia (16.7).[23] This finding is in agreement with the data reported in literature, which accounts for the shift to a higher binding energy for hafnium in a Hf–O–Si environment with respect to pure HfO_2.[24] Accordingly, the values detected for the $Hf4d_{5/2}$ peak, in the range 214.0–214.6 eV, are also higher than the value reported in literature (213.2 eV).[11,24]

The in-depth composition of the films, performed by sputtering analysis cycles, reveals an even distribution of the hafnium guest species in the silica host matrix. As shown in Figure 11, where the Si/Hf atomic ratios are plotted versus the sputtering time, the hafnium signal displays a uniform profile along the investigated thickness. In the outer layers, an enrichment of silicon was detected, whereas after about 20 min of sputtering the amount of hafnium gradually started to increase and the experimental Si/Hf atomic ratio ranged from 5 to 9.5, with a mean value of about 8, which is in good agreement with the nominal ratio in the starting solution (7.2). After 480 min of sputtering, the boundary between the film and the silicon substrate was reached, as the silicon peak displays two fully distinguishable components: the first at 103.9 eV, which is ascribable to the silica film, and the second at about 99.5 eV, which is attributable to the metallic silicon of the wafer substrate.

From the carbon signal, a considerable reduction in the contamination was observed after sputtering, but a significant presence of carbon (about 10% atomic) was detected along the whole film thickness, which can be ascribed to incomplete decomposition of organics upon annealing.

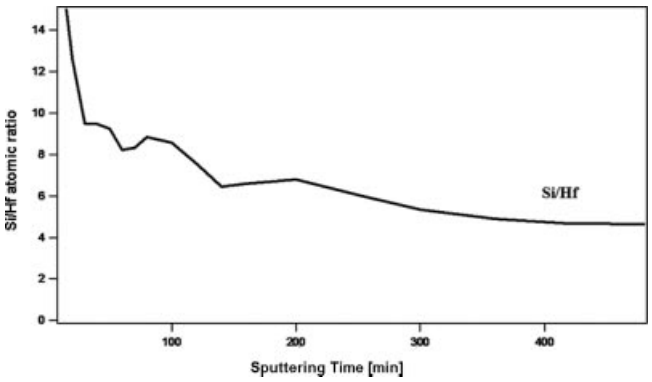

Figure 11. XPS in-depth distribution of the Si/Hf ratio.

Conclusions

We demonstrated an effective, direct synthetic method for the preparation of mesostructured hafnium oxide doped silica films by the use of a decaethyleneglycol hexadecyl ether/hafnium butoxide complex as a structure-directing agent. By variation of the ratio between the modified surfactant:silica precursor, face-centred orthorhombic, 2D-centered rectangular and lamellar films were obtained. The influence of heat treatment on the mesostructure was investigated by GISAXS and TEM measurements. The face-centred orthorhombic mesostructure was stable at temperatures above 700 °C. The 2D-centered rectangular structure showed a somewhat lower heat stability and was already affected at that temperature. The lamellar structure was destroyed at 300 °C. The in-depth chemical composition of the film was analyzed by XPS. The measurements showed that there is a uniform distribution of the hafnium species in the silica host matrix with a concentration close to the nominal value in the starting solution.

Experimental Section

Materials: Hafnium *n*-butoxide was supplied from Aldrich and used without further purification. Tetraethyl orthosilicate and Brij-56 ($C_{16}EO_{10}$) were purchased from Fluka and used as received. Toluene (99%) was obtained from Merck and distilled from calcium hydride prior to use. Ethanol (96%) was supplied by Merck.

Methods: The composition of the films at the surface and in the bulk was investigated by XPS. Photoelectron spectra were obtained with a Perkin–Elmer Φ5600ci spectrometer by using nonmonochromatized Al-K_α radiation (1486.6 eV). The spectrometer was calibrated by assuming the binding energy (BE) of the Au4f7/2 line at 83.9 with respect to the Fermi level. The standard deviation for the BE values was 0.15. The reported BE were corrected for charging effects by assigning the BE value of 284.6 eV to the C1s line of carbon. Survey scans (187.85 pass energy, 1/step, 25 ms/step) were obtained in the 0–1300 range. Detailed scans (58.7 pass energy, 0.2 eV/step, 50 ms/step) were recorded for the O1s, C1s, Hf4f, Hf4d and Si2p regions. The atomic percentages of the different species were determined by using the C1s, O1s, Hf4f and Si2p regions. In particular, after each sputtering cycle, the determination of the four atomic percentages was performed as a function of the increasing sputtering time, which was used to obtain the in-depth profiles of the various species. The atomic composition, after a Shirley-type background subtraction was evaluated by using sensitivity factors supplied by Perkin–Elmer.[23,25] Depth profiles were carried out by Ar^+ sputtering at 3 keV with an argon partial pressure of 5×10^{-6} Pa. A specimen area of 2×2 mm^2 was sputtered. Samples were introduced directly by a fast entry lock system into the XPS analytical chamber. The assignment of the peaks was carried out by using the values reported.[23,24,26] Room-temperature grazing incidence GISAXS experiments were performed at the Austrian high-flux SAXS beam line at the synchrotron radiation centre Elettra, Trieste, Italy.[27] Films deposited on single-side polished silicon wafer substrates and subsequently calcined at different temperatures were measured at a photon energy of 8 keV and with a grazing angle α below 2° between the beam and the film surface. 2D-diffraction patterns were recorded with a CCD detector (Photonic Science) with a distance (L) of 107 cm from the sample. The recorded area is indicated by the dotted rectangle in Figure 12. The d spacing was determined from the diffraction spots by analysis of the CCD images with the FIT2D program (A. P. Hammersley/ESRF). TEM images were recorded with a JEOL JEM-100CX analytical transmission electron microscope. For film samples, the surface of the film was scratched and the powder was attached to Formvar copper grids. XRD patterns were recorded with a Philips X'Pert diffractometer with a Philips PW 3040/60 (mppx) generator and a Philips PW 3050/60 goniometer. NMR spectra were recorded with a Bruker Avance 300 spectrometer equipped with a 5 mm broadband probe head and a z gradient unit. 2D spectra, COSY (correlated spectroscopy), TOCSY [totally correlated spectroscopy, T(mix) = 120 ms] and HSQC (heteronuclear single quantum correlation), were measured with Bruker standard pulse sequences. $CDCl_3$ (99.8% euriso-top) was employed as the solvent.

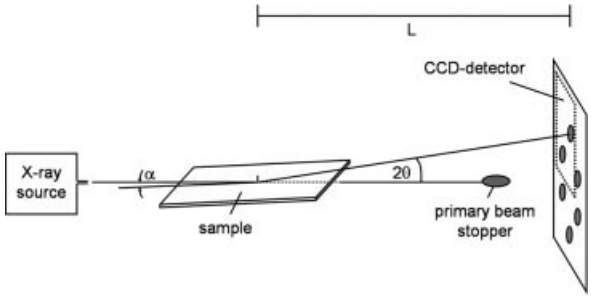

Figure 12.Setup of the GISAXS measurements.

Synthesis of Hf-Brij56: The reaction was carried out in a three-necked round-bottomed flask equipped with a reflux condenser and a distillation apparatus under an argon atmosphere. To remove residual water, the surfactant Pluronic-P123 was dissolved in toluene and heated to 100 °C for approximately 4 h. During that time, the toluene/water azeotrope was distilled off. The dried surfactant was then dissolved again in fresh absolute toluene. $Hf(OBu)_4$ was also dissolved in absolute toluene and added dropwise to the above prepared solution with a transition metal/surfactant molar ratio of 1:1. The mixture was stirred at 110 °C overnight. Toluene and the formed alcohol were removed by distillation and the metal-coordinated surfactants were obtained as slightly yellow or white pastes in 95% yield. ^{1}H NMR (300.13 MHz, $CDCl_3$): δ = 0.82–0.95 (m, 12 H, 1-H, 14-H), 1.22–1.4 (m, 32 H, 2-H, 11-H, 12-H, 13-H), 1.55 (m, 8 H, 10-H, 3-H), 3.42 (t, J = 6.8 Hz, 2 H, 9-H), 3.61 (m, 38 H, 6-H, 7-H, 8-H), 4.05 (m, 6 H, 4-H), 4.20 (m, 2 H, 5-H) ppm. ^{13}C NMR (75.47 MHz, $CDCl_3$): δ = 14.2 (C-1, C-14), 19.1 (C-2), 22.8 (C-13), 26–32 (C-11, C-12), 29.5 (C-10), 36.8 (C-3), 69.3 (C-4), 69.2 (C-5), 70.0 (C-6), 71.7 (C-9), 70–71 (C-7, C-8) ppm.

Film Preparation: TEOS (61 mL) was prehydrolyzed in a solution containing water (4.87 mL), dilute hydrochloric acid (0.07 N, 2 mL) and ethanol (61 mL) at 60° for 90 min. This "stock" solution (8 mL) was mixed with ethanol (7 mL), HCl (0.07 N, 0.4 mL), water (0.4 mL) and different amounts of the metal-coordinated surfactant resulting in a molar ratio of Hf–Brij/TEOS/EtOH/H_2O/HCl = *x*:1:42:15:0.0052. Films were prepared within one hour on single-sided polished silicon wafers by dip-coating with a holding time of 30 s, a withdrawal speed of 4 mm/s at a relative humidity of 35–50%. The films were aged for at least 24 h prior to calcination. Powder samples for XRD analysis were scratched from coated glass plates after drying for 24 h at room temperature.

Acknowledgments

The financial support of the European community for the ELETTRA synchrotron measurements is greatly acknowledged. We thank the USTEM at the Vienna University of Technology for allowing access to their TEM facilities and Berthold Stäüger from the Division of Structural Chemistry of the Institute of Chemical Technologies and Analytics, Vienna University of Technology for the XRD measurements.

[1] R. G. Simhan, *J. Non-Cryst. Solids* **1983**, *54*, 335–343.
[2] A. Paul, *J. Mater. Sci.* **1977**, *12*, 2246–2268.
[3] X. Song, A. Sayari, *Catal. Rev. Sci. Eng.* **1996**, *38*, 329–412.
[4] P. Liu, J. Liu, A. Sayari, *Chem. Commun.* **1997**, 577–578.
[5] P. Yang, D. Zhao, D. I. Margolese, B. F. Chmelka, G. D. Stucky, *Chem. Mater.* **1999**, *11*, 2813–2826.
[6] T. Brezesinski, B. Smarsly, K. Iimura, D. Grosso, C. Boissiere, H. Amenitsch, M. Antonietti, C. Sanchez, *Small* **2005**, *1*, 889–898.
[7] L. Malfatti, T. Kidchob, S. Costacurta, P. Falcaro, P. Schiavuta, H. Amenitsch, P. Innocenzi, *Chem. Mater.* **2006**, *18*, 4553–4560.
[8] Y. S. Lin, R. Puthenkovilakam, J. P. Chang, *Appl. Phys. Lett.* **2002**, *81*, 2041–2043.
[9] G. D. Wilk, R. M. Wallace, J. M. Anthony, *J. Appl. Phys.* **2000**, *87*, 484–492; G. D. Wilk, R. M. Wallace, *Appl. Phys. Lett.* **1999**, *74*, 2854–2856; G. D. Wilk, R. M. Wallace, *Appl. Phys. Lett.* **2000**, *76*, 112–114.
[10] J. P. Maria, D. Wickaksana, J. Parrette, A. I. Kingon, *J. Mater. Res.* **2002**, *17*, 1571–1579.
[11] L. Armelao, D. Bleiner, V. Di Noto, S. Gross, C. Sada, U. Schubert, E. Tondello, H. Vonmont, A. Zattin, *Appl. Surf. Sci.* **2005**, *249*, 277–294; L. Armelao, H. Bertagnolli, D. Bleiner, M. Groenewolt, S. Gross, V. Krishnan, C. Sada, U. Schubert, E. Tondello, A. Zattin, *Adv. Funct. Mater.*; DOI: 10.1002/adfm.200600458; L. Armelao, C. Eisenmenger-Sittner, M. Groenewolt, S. Gross, C. Sada, U. Schubert, E. Tondello, A. Zattin, *J. Mater. Chem.* **2005**, *15*, 1838–1848.
[12] K. V. Terry, C. G. Lugmair, T. D. Tilley, *J. Am. Chem. Soc.* **1997**, *119*, 9745–9756.
[13] D. A. Neumayer, E. Cartier, *J. Appl. Phys.* **2001**, *90*, 1801–1808.
[14] C. J. Brinker, Y. Lu, A. Sellinger, H. Fan, *Adv. Mater.* **1999**, *11*, 579–585.
[15] D. J. Mitchell, G. J. T. Tiddy, L. Waring, T. Bostock, M. P. McDonald, *J. Chem. Soc., Faraday Trans. 1* **1983**, *79*, 975–1000.
[16] P. C. A. Alberius, K. L. Frindell, R. C. Hayward, E. J. Kramer, G. D. Stucky, B. F. Chmelka, *Chem. Mater.* **2002**, *14*, 3284–3294.
[17] R. Supplit, N. Hüsing, H. Bertagnolli, M. Bauer, V. Kessler, G. A. Seisenbaeva, S. Bernstorff, S. Gross, *J. Mater. Chem.* **2006**, *16*, 4443–4453; N. Huesing, B. Launay, G. Kickelbick, S. Gross, L. Armelao, G. Bottaro, M. P. Feth, H. Bertagnolli, G. Kothleitner, *Appl. Catal. A* **2003**, *254*, 297–310.
[18] D. Grosso, F. Cagnol G. J. de A. A. Soler-Illia, E. L. Crepaldi, H. Amenitsch, A. Brunet-Bruneau, A. Bourgeois, C. Sanchez, *Adv. Funct. Mater.* **2004**, *14*, 309–322.
[19] S. Besson, C. Ricolleau, T. Gacoin, C. Jacquiod, J.-P. Boilot, *Microporous Mesoporous Mater.* **2003**, *60*, 43–49.
[20] P. Falcaro, D. Grosso, H. Amenitsch, P. Innocenzi, *J. Phys. Chem. B* **2004**, *108*, 10942–10948.
[21] M. Klotz, P.-A. Albouy, A. Ayral, C. Menager, D. Grosso, A. van der Lee, B. Cabuil, F. Babonneau, C. Guizard, *Chem. Mater.* **2000**, *12*, 1721–1728.
[22] R. C. Hayward, P. C. A. Alberius, E. J. Kramer, B. F. Chmelka, *Langmuir* **2004**, *20*, 5998–6004.
[23] K. W. Terry, C. G. Lugmair, T. D. Tilley, *J. Am. Chem. Soc.* **1997**, *119*, 9745–9756.
[24] F. Moulder, W. F. Stickle, P. E. Sobol, K. D. Bomben, *Handbook of X-ray Photoelectron Spectroscopy*, Perkin–Elmer Corporation, Eden Prairie, MN, **1991**.
[25] V. Cosnier, M. Olivier, G. Theret, B. André, *J. Vac. Sci. Technol.* **2001**, *19*, 2267–22710.
[26] D. A. Shirley, *Phys. Rev.* **1972**, *5*, 4709–4714.
[27] D. Briggs, M. P. Seah, *Practical Surface Analysis*, John Wiley & Sons, New York, **1990**.
[28] H. Amenitsch, M. Rappolt, M. Kriechbaum, H. Mio, P. Laggner, S. Bernstorff, *J. Synchrotron Radiat.* **1998**, *5*, 506–508.

Received: March 11, 2007
Published Online: May 25, 2007

